La mer 30: 287–296, 1992
Société franco-japonaise d'océanographie, Tokyo

Mesoscale coherent structures in the surface wind field during cold air outbreaks over the Far Eastern seas from the satellite side looking radar

Leonid M. MITNIK*

Abstract: Winter monsoon over the Far Eastern seas is followed by regular cold air outbreaks from Asia. Convection developed in the process manifests itself in a form of cloudiness on the satellite optical images and often shows the diverse mesoscale coherent structures: rolls, open and closed cells, vortex and chains of vortices. In such situations a peak appears between turbulent and synoptic peaks in a horizontal wind speed power spectrum. The mesoscale organized structures are also revealed in the sea surface wind W (surface roughness) field, which is observed from analysis of the images, obtained by the side looking radar from "Okean" series satellites. In the present paper the normalized radar cross section (NRCS) is calculated for two-scale model of W distribution in open and closed cells with variations of synoptic and mesoscale wind, the angle between a radar sensing plane and a synoptic wind vector, etc. The model distributions of the NRCS are in good agreement with the brightness variations within the cells on the radar images. The probable detection of the mesoscale organized structures in the subsurface layer of the ocean as a reseponse to quasiperiodic atmosphieric forcing will have a special importance in future experiments.

1. Introduction

During the winter monsoon, the cold air outbreaks are the typical features of the meteorological regime of the Far Eastern seas. These outbreaks are the most severe in the world. The passage of cold, low-humidity air over the warm waters induces strong latent, sensible, and radiative heat fluxes at the air-sea interface reaching 1000–12000 W/m^2 at high wind speeds and clear skies (AGEE, 1987).

During such outbreaks characteristics of the ocean and atmosphere change significantly: surface waters cool down and become more saline and the boundary layer of the atmosphere gets warm and loses its stability (HUH *et al.*, 1984). As a result, the mesoscale organized convective motions are formed in the atmosphere. They are manifested, in particular, in the surface wind field.

* Pacific Oceanological Institute, Far Eastern Branch, Russian Academy of Sciences, 43 Baltiyskaya Street, 690041 Vladivostok, Russia

It is known that mesoscale variabilities of the surface wind and derived surface fluxes may be important in predicting and explaining the rapid development of marine cyclones and the associated large flux variations (NUSS and BROWN, 1987). The mesoscale wind variations can change a structure of the ocean upper layer significantly. Using measurements from the system of moored buoys, TRUMP *et al.* (1982) found out that ocean temperature and current fluctuations at a depth of 20 m are significantly correlated with mesoscale atmospheric structures associated with the passage of well developed cells. As discussed by FEDOROV and GINSBURRG (1984), it is impossible to explain this correlation by using experimental meteorological data by TRUMP *et al.* (1982) and model calculations. On the other hand, ORLANSKI and POLINSKY (1983), using their model, determined that mesoscale atmospheric forcing is potentially an important source for the observed 100 km-scale variability in the ocean. As suggested by MONIN *et al.* (1987), coherent structures in the atmospheric boundary layer may account

for the horizontal mesostructures in the main thermocline. The necessity of considering the mesoscale wind variability follows also from a work by D'ASARO (1988).

Clouds are the obvious products of the large fluxes from the ocean to the atmosphere during cold air outbreaks. At first they have a shape of cloud rolls and then they are converted gradually to cells. Cloud patterns on the visible and infrared (IR) satellite images show synoptic, subsynoptic and mesoscale structures, and, together with the brightness temperature of cloudiness and cloudless regions of the ocean, give a certain representation about conditions on the upper boundary and inside the convective marine boundary layer.

Since September 1983 when the first satellite with a side-looking radar (SLR) was launched (MITNIK and VIKTOROV, 1990), the opportunities to investigate processes in the marine boundary layer have broadened because the surface wind field can be estimated from radar data. Such radars were installed on the Okean series satellites (Kosmos-1500, Kosmos-1766, Okean and others). They operate at wavelength of 3.15cm with vertical polarization. A ground resolution is 2.1–2.8 km (in flight direction) by 0.8–3 km (normal to flight) at 650 km altitude. A swath width is about 460 km. The angle of incidence changes from 21° to 46° within the swath.

The purpose of this study is to evaluate the possibility of the satellite SLR images of the ocean for representing the mesoscale structures in the surface wind field. The main evidence on horizontal wind variations during mesoscale cellular convection is described in section 2. Coupling of the brightness distribution within open and closed cells on the radar images with the sea surface wind characteristics is considered in section 3. Conclusion and proposal on a special experiment to study the mesoscale processes in the air-sea system are presented in section 4.

2. Mesoscale horizontal wind variations

Fig. 1 shows visible and radar images of the Sea of Okhotsk and an area south off the Kuril Islands obtained by Kosmos-1766 satellite. Cloud field (Fig. 1a) of Meteor-2 visible image is an indicator of organized convection, which takes the form of streaks (area 1), open cells (area 2), chains of vortices (areas 3 and 4). Such forms of the convection are typical in winter monsoon period when cold air masses from Asia move over the warmer Pacific Ocean surface (TRUMP *et al.*, 1982; AGEE, 1987; MITNIK and VIKTOROV, 1990).

The radar sensing of the ocean (Fig. 1b) had been carried out half an hour before the visible survey (Fig. 1a). Swath boundaries of the SLR are depicted in Fig. 1a by solid lines. The main cause of changes in brightness is the sea surface roughness (surface wind) variability. The increase of the sea surface wind results in the increase of the radar image brightness. Brightness distribution suggests that there should be a tight correlation between roughness and cloudiness, between processes on lower and upper boundaries of the boundary layer of the atmosphere. For example, bands of alternating brightness in area 1 (Fig. 1b) have the same orientation as cloud streaks in Fig. 1a. The mesoscale brightness variations caused by air circulation inside individual cells are well visible in area 2. Similar formations are prominent in zone 5 with weak winds. Bands join cyclonic vortex of chain 3. Maximum wind speed (about 10–15 m/s in accordance with surface weather map) is observed in the area where clouds are denser and brighter. Zone with maximum wind speed is located under the cloud spiral near its internal boundary, and has a width of about 30–35 km. To the north of the cloud vortex wind speed is markedly lower.

In the region of chain 4 speed of northwest wind was 7–10 m/s by ship data. Dimensions of individual vortices in the chain and distances between their centers are 30–35 km. The southwest boundary of the vortices has prominent radar contrast against the background (area 6 with low wind speed located to the south). The boundary of radar contrast corresponds to the northeast edge of the cloud vortices. Their dimensions increase downwind. Thus, from the analysis of this radar image it follows that the diverse mesoscale organized structures are observed in the sea surface wind.

Taking into account the spatial resolution of the SLR, the primary attention will be given to the domain of atmospheric motions with spatial

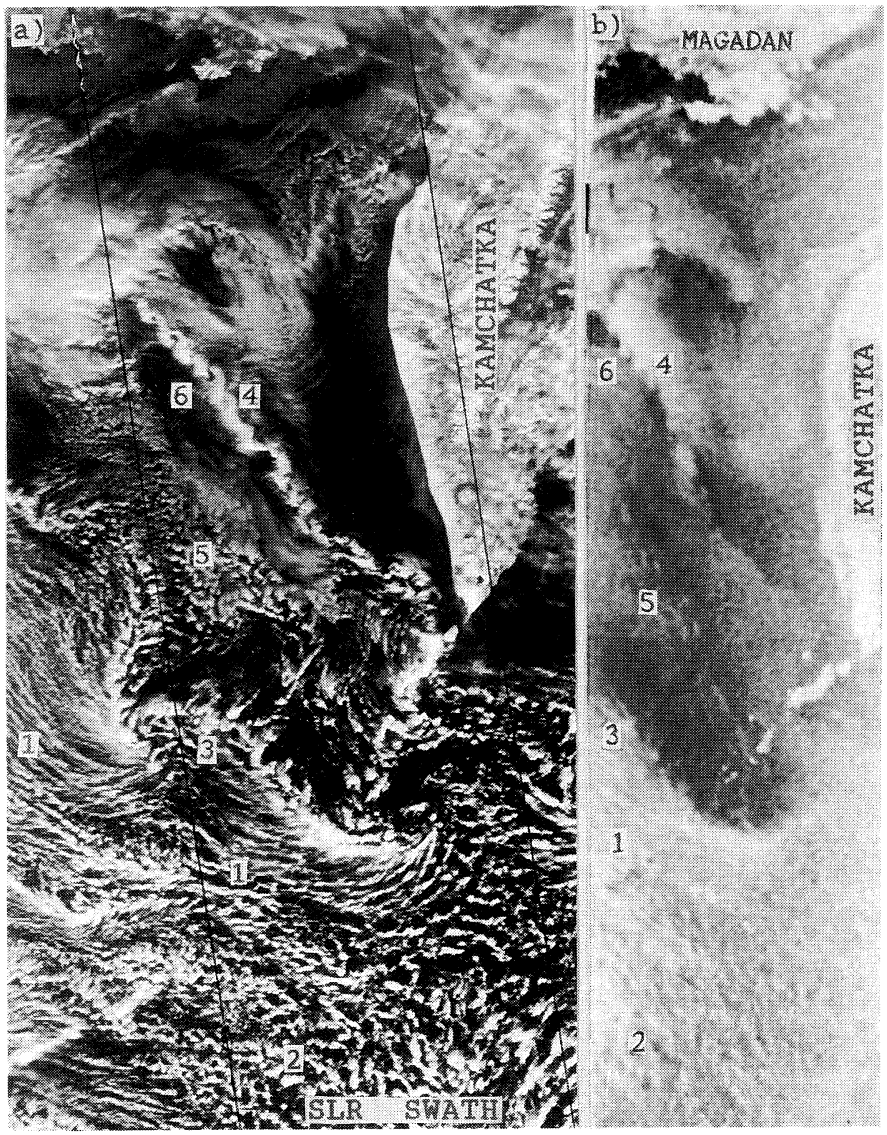

Fig. 1. (a) Meteor-2 visible image and (b) Kosmos-1500 SLR image (3 Jan. 1985, about 0100 GMT) of the Sea of Okhotsk and the Pacific Ocean south of Kuril Islands.

scales L between 1–3 and 100 km and time scales T of minutes to hours. At higher frequencies f ($=1/T$) Kolmogorov turbulence takes place, and at lower ones the synoptic scale motions including fronts and depressions take place. These large-scale structures can be investigated by both scatterometer and SLR.

Our ability to resolve the mesoscale wind variability in the marine boundary layer remains limited by the insufficient temporal and spatial resolution and accuracy of data. A study by NUSS and BROWN (1987) indicates that in data-rich regions, routine surface observations are separated by roughly 400 km on the average and by even greater distances in data-sparse regions. The major sources of the observations are wind reports from ships of opportunity. However, a comparison of wind data from ships and buoys revealed the poor quality and unreliability of wind reports by ships (PIERSON,

1990). Eventually, satellite instruments such as scatterometers and microwave radiometers may provide an observational base for more detailed and accurate surface data for scales larger than 20–50 km. The wind variations with smaller scales will be spatially integrated in the footprint of a satellite sensor. As a result of smoothing, additional errors in the surface wind estimation can arise, which would, in turn, produce poor quality of weather and wave forecasts (PIERSON, 1983, 1990).

The spatial resolution of the satellite SLR permits us to investigate the surface wind variability with scales of 2–50 km. It is of particular importance because the characteristic scales of a major part of coherent motions in the atmosphere are in these limits (AMBROZI *et al.*, 1973; VETLOV and VEL'TISHCHEV, 1982; MITNIKand V IKTOROV, 1990).

Let us summarize briefly the data on the horizontal wind spectrum. As was first shown by VAN der HOVEN (1957), there is a so-called "spectral gap" between turbulent and synoptic peaks in the wind speed power spectrum over land. Then the existence of the gap was revealed in spectra of marine winds (ISHIDA *et al.*, 1984; ISHIDA, 1989; CHAMPAGNE-PHILIPPE, 1989). The existence of the low, flat energy area of spectral gap denotes that energy sources in the corresponding frequency range were lacking during measurements.

A different situation arises when organized convective mesoscale patterns such as rolls, open and closed cells are observed in the atmosphere. Spectrum form changes: secondary peaks may be observed in the gap region between 0.5 and 1.5 hours. In particular, such peaks were found in the wind spectra, obtained from buoys moored in the East-China Sea during the Air Mass Transformation Experiment (AMTEX '75) (BURT and AGEE, 1977; TRUMP *et al.*, 1982; ISHIDA *et al.*, 1984). The meteorological measurements were performed at the height of 4.3 m. Fig. 2 shows two wind spectra, averaged from six buoys. The vertical axis is a frequency multiplied by energy density and the horizontal one is a frequency in logarithmic scale. The lower curve characterizes a typical situation with the spectral gap and the upper one represents a spectrum in the passage of the closed mesoscale

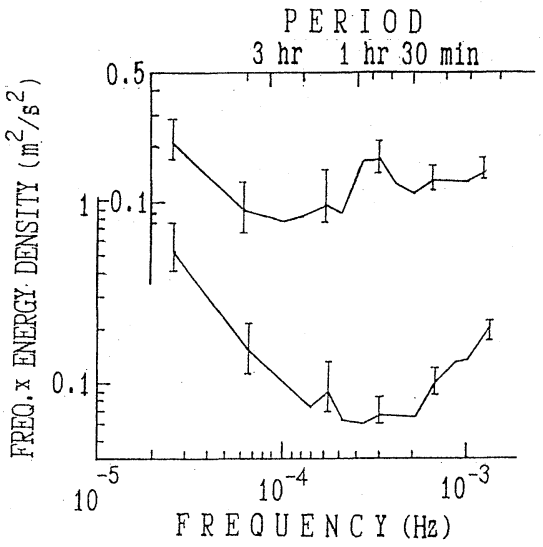

Fig. 2. The averaged spectra of wind speed for six buoys for periods of the well organized MCC (0840 GMT, 16 Feb. – 0555 GMT, 17 Feb. 1975) (upper curve) and of dissipating MCC and without cells, 1150 GMT 17 Feb. – 0955 GMT 18 Feb. 1975) (lower curve) (ISHIDA et al., 1984).

convective cells with average diameter of 24–30 km. A peak at $T = 1$ hr is marked well. Bars correspond to 80 % confidence interval (ISHIDA *et al.*, 1982). Processing of data from buoys located in the triangle apices showed the existence of divergent and convergent air flows corresponding to closed circulation system; downward motion and clear skies in the cell periphery with upward motion and clouds at its center (ISHIDA *et al.*, 1984). A model of the representative closed cell based on the data for 30 hrs period of strong cellular development was characterized by fluctuations in air temperature (±0.2℃), humidity (±0.2 g/kg), and horizontal wind speed (±0.5 m/s relative to the average value of 8 m/s) (TRUMP *et al.*, 1982).

High coherence (0.9) between wind speed and air temperature with the phase difference of about 170° was also revealed by ISHIDA (1989) when significant peaks in their spectra occurred simultaneously in the mesoscale range at a period of 30–40 min (Fig. 3). The data were obtained from an array of buoys during the JASIN-1978 field experiment in the northwest of Scotland. The coherence and phase shift may have been caused by some form of mesoscale

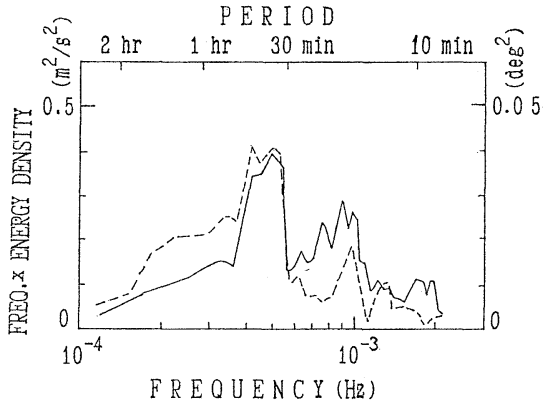

Fig. 3. Spectra of wind speed (solid line) and air temperature (dotted curve) from buoy B3 for 14 21.5 GMT on Aug. 1978 (ISHIDA, 1989).

convective structures.

The spectrum of the horizontal wind measured on the coast during cold air outbreak also showed a somewhat significant peak of energy centered around 0.5–1hr. Wind had been observed for 53 hrs when cumulus and cumulonimbus clouds were numerous and, most of the time, were organized in open mesoscale cells (CHAMPAGNE-PHILIPPE, 1989).

The mesoscale convective cells (MCC) have typical diameters of 10–100 km. Magnitude of the sea surface wind variations may be much larger than the average value reported by TRUMP *et al.* (1982). For example, wind fluctuations up to ±3–4 m/s were registered by onboard sensors, when an aircraft crossed a cellular convection area over the Pacific Ocean at low levels (50 and 90m) (OVERLAND and WILSON, 1984). Wind speed of mesoscale circulation within the large open convective cells may reach 10 m/s and more at their formation (AMBROZI *et al.*, 1973). The average wind speed during mesoscale convection over the Pacific Ocean obtained from the analysis of the satellite cloud images and ship reports was 8.6 m/s at closed cells, 14.3 m/s at open cells, and 17.6 m/s in the case when the cells have crescent shape (POKHIL, 1985).

3. Manifestation of mesoscale cellular convection on radar images of the ocean

The analysis of satellite optical and radar images shows that the mesoscale convective cells

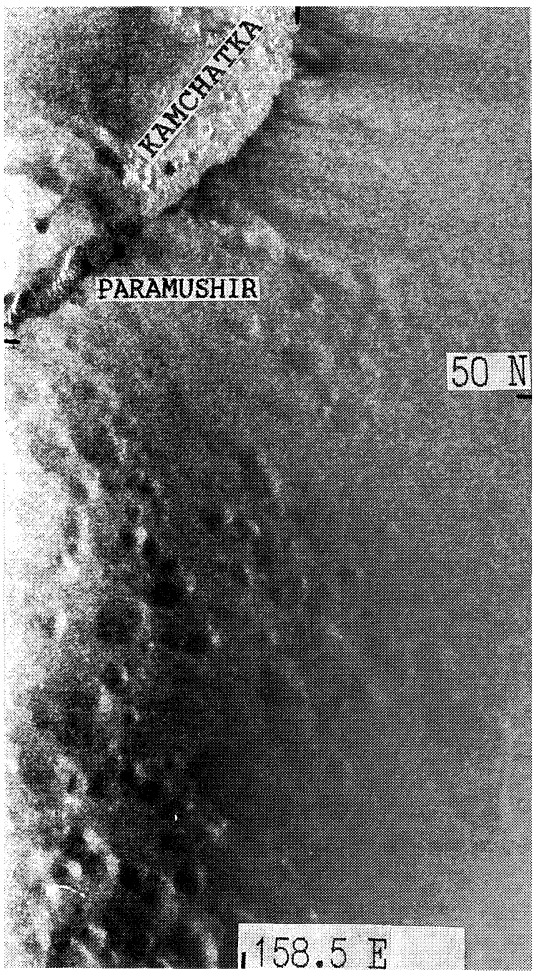

Fig. 4. Okean SLR image of the Pacific Ocean south of Kamchatka for 1940 GMT, 16 Nov. 1988.

are the most popular organized structures in the atmosphere over the ocean in winter period. By means of buoy, ship and aircraft measurements it is difficult or impossible to study the mesoscale spatial structures of wind field in detail. At the same time, the sea surface wind distribution is reflected distinctly on the radar images.

The individual convective cells are well seen in the brightness (roughness) field on the radar image in Fig. 4. During radar survey a synoptic situation was characterized by a deep cyclone with a minimum pressure of 985 mb. Its center was located over the northeastern part of the Sea of Okhotsk outside the swath. A northwest

and west wind speed ranged between 5 and 17 m/s. The surface imprints of the individual cells have mainly circular form. Their diameters change from 10 to 40 km. At higher wind speed these imprints take an stretched form. The effect of air circulation within the cell appears as dark and light zones. A number of cells have crescent brightness distribution: a dark patch surrounded by light sickle. As a result, outlines of the cell have positive, negative or close to zero contrast against the background.

To explain these features the model calculations of the normalized radar cross section (NRCS) σ° of the sea surface have been carried out for horizontal wind distributions in open and closed cells. The brightness of the radar image is proportional to σ°. The value of NRCS is a characteristics of scattered signal power and related to the wind speed W by power law (MOORE and FUNG, 1979; MASUKO *et al.*, 1986).

$$\sigma^\circ(\lambda, p, \theta, \phi) = 10[G(\lambda, p, \theta, \phi) + H(\lambda, p, \theta, \phi)\lg W], \quad (1)$$

where λ is radar wavelength, p polarization of signal, θ angle of incidence, ϕ azimuthal angle (angle between the plane of radar signal propagation and the direction opposite to the wind vector), G coefficient and H wind speed exponent. With the increase of θ the values of σ° decrease.

Azimuthal relationship is approximated well by the cosine expansion regression:

$$\sigma^\circ = A_0 + A_1 \cos\phi + A_2 \cos 2\phi. \quad (2)$$

Empirical approximate coefficients $G(\theta, \phi)$, $H(\theta, \phi)$, A_0, A_1 and A_2 for $\lambda = 3$ cm obtained by MASUKO *et al.* (1986) have been used in subsequent calculations of σ° at vertical polarization.

The features of NRCS distribution within the MCC are explained by using a simple two-component model for horizntal wind pattern (MITNIK and VIKTOROV, 1990). There is a synoptic (background) flow with constant wind speed W_s and regular mesoscale cellular circulation imposed on it. The circulation in cells is axisymmetrical with magnitude W_c. The function $W_c(r)$ describing dependence of wind speed on the distance r from the center of a cell is

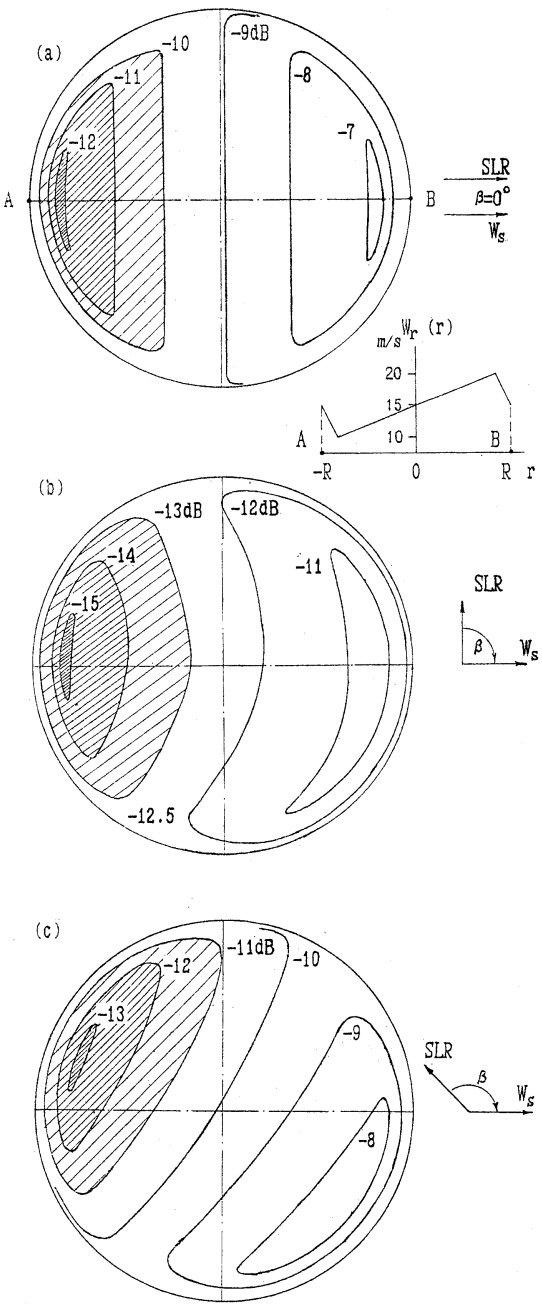

Fig. 5. Distributions of NRCS (in dB) inside open cell for $W_s = 15$ m/s, $W_c = 5$ m/s, $\theta = 30°$: (a) $\beta = 0°$, (b) $\beta = 90°$, and (c) $\beta = 135°$.

specified analytically or numerically. Resulting wind speed $W_r(r)$ and the angle $\phi(r)$ in any point within the cell are determined from given

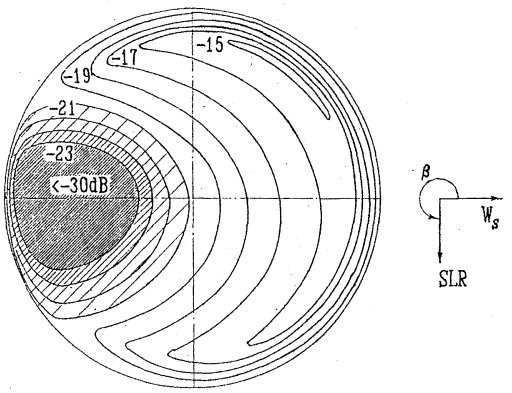

Fig. 6. Distributions of NRCS (in dB) inside open cell for $W_s=5$ m/s, $W_c=5$ m/s, $\theta=30°$, $\beta=270°$.

values of W_s, $W_c(r)$, and β (angle between W_s and the radar signal plane). Angle θ is found from the known position of the cell inside the SLR swath. It allows us to use relationships (1) and (2).

The model calculations of $\sigma°$ distribution have been carried out at wavelength of 3 cm with vertical polarization for $W_s=0-15$ m/s, $\beta=0-360°$, $\theta=30-40°$ and different $W_c(r)$ functions.

For the open cell (upward motion in the cell periphery with downward motion at the center) horizontal wind speed is directed from the center toward the periphery and given by a function

$$W_c(r)=\begin{cases}(|r|/R)W_c, & 0<r<r_0,\\ [(R-|r|)/(R-r_0)]W_c, & r_0<r<R,\end{cases}$$

where $W_c=0.5-5$ m/s, $r_0=5R/6$, and R is the radius of the cell. The origin is at the cell center.

For cell with $R<10$ km change of an angle θ within the cell is small and can be neglected. For such cells the values of $\sigma°$ at the center and the cell edge are equal to each other and determined by parameters of W_s, β and θ.

Radar patterns of the open MCC are shown in Figs. 5 and 6. The extremes of the NRCS are located at a distance of $r=r_0$. Here the resulting wind approaches the extremal values W_{ext} in those points where a mesoscale flow is added with synoptic one or subtracted from it, as shown for A–B section in Fig. 5a. A position of the NRCS extremes may, however, differ from the points of W_{ext} due to the impact of azimuthal dependence (2) (Fig. 5). Amplification of mesoscale circulation (growth of W_c) at W_s=const. will increase the radar contrast between different parts of the cell.

The radar patterns of the MCC significantly depend on the orientation of the radar sensing plane relative to background flow (on angle β). In particular, isolines of $\sigma°$ are of a concave shape when β is near $\pm 90°$ (Fig. 5b). In such cases the radar images of the MCC take crescent shape (KALMYKOV *et el.*, 1985; MITNIK and VIKTOROV, 1990). At other values of β the concavity is small, if any (Figs. 5a and 5c).

As the speed of synoptic flow decreases the values of $\sigma°$ decrease, too, and the radar patterns of the MCC are transformed. The edges of sickles are twisted towards the wind (Fig. 6). In real conditions differencies in the brightness inside the cell may be even greater, when the resulting wind speed will be lower than a threshold value W_0 (which depends on the sea surface temperature). At $W_r<W_0$ capillary-gravity waves on which the radar signals are scattered are not formed (DONELAN and PIERSON, 1987) and appropriate parts of the cells become dark. The dark patches in windward parts of the open cells give a higher radar contrast of leeward ones where synoptic and mesoscale flows are added (Fig. 4).

The mesoscale circulation in the closed cell was described by a harmonic function (TRUMP *et al.*, 1982)

$$W_c(r)=-W_c\sin(\pi r/R).$$

Horizontal wind speed is directed from the cell periphery toward its center. The origin is again at the cell center.

Distributions of NRCS for the closed MCC with $W_c=5$ m/s are presented in Fig. 7. Vector diagrams give an indication of resulting horizontal wind vector for four points located at a distance of $r=R/2$ where $W_c(r)$ has a maximum. Inside the closed cell there are areas having positive and negative radar contrast against the background. The contrast magnitude and radar patterns of the cell depend significantly on the relationship between W_s, W_c and β, and also on a number of other parameters.

For large MCC ($R>10$ km) the change of an angle θ within the cell must be allowed for in model calculations. To illustrate, the additional

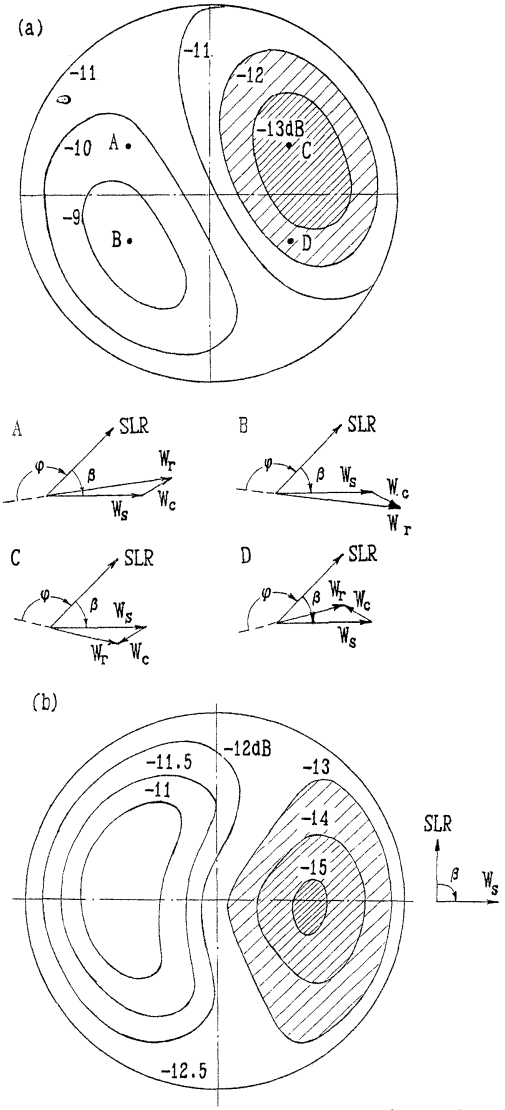

Fig. 7. Distributions of NRCS (in dB) inside closed cell for W_s=15 m/s, W_c=5 m/s, θ =30°: (a) β =45°, (b) β =90°.

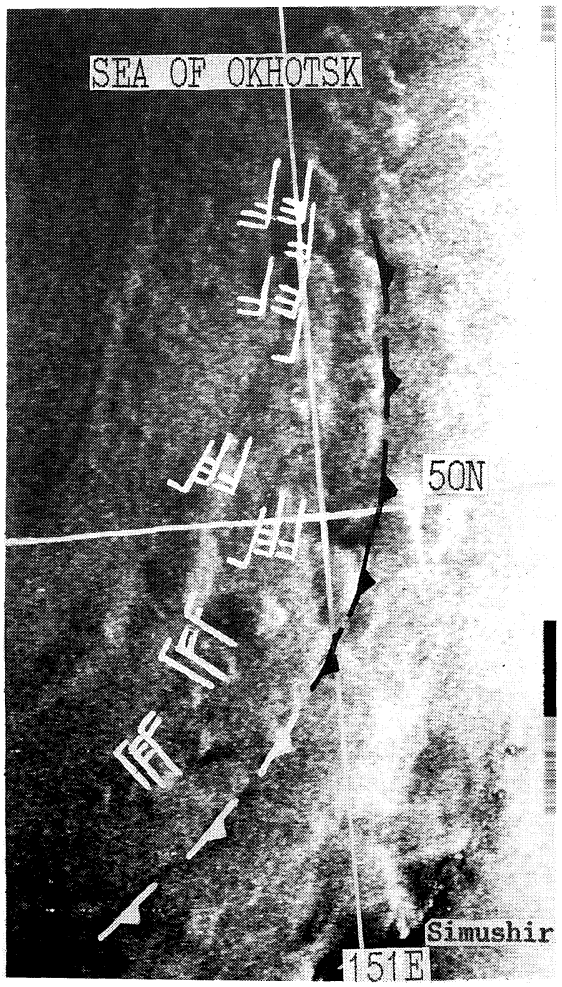

Fig. 8. Okean SLR image of the central part of the Sea of Okhotsk for 1245 GMT, 14 Oct. 1988, and the retrieved average and extremal values of the surface wind vector in a cell area (Bukharov et al., 1991).

decrease of σ° value of remote (from the SLR) portion of the cell relative to near one will be 1.0–1.6 dB for cells with R=20 km at θ =30–40° (MITNIK and VIKTOROV, 1990).

Let us correlate the results of model calculation with the features of the brightness (surface wind) distribution in areas of cell convection on the radar images. An algorithm of wind speed determination by radar image was described by MITNIK and VIKTOROV (1990). This algorithm takes into account the information on radar system, calibration of a transmitter power, altitude of the satellite, wind direction (from surface weather maps), values of an angle of incidence for the ocean area under investigation, etc. Let us analyze the radar image of the south part of the Sea of Okhotsk obtained by "Okean" satellite (Fig. 8a, BUKHAROV *et al.*, 1991). By the time of the radar survey this area had been influenced by the secondary cold front which was formed in the rear of the occluded cyclone. This front moved rapidly to the east with a

speed of 6 m/s in the northern part and 11 m/s in more active southern one. The air temperature near the sea surface behind the cold front was 1.5–2℃ lower than before it.

The larger part of the cells is organized in a form of chains stretched northeastward (lower part of the image) and northward (upper one) along the front line. The cells form is nearly circular, but their dimensions are distinguished significantly (from 12 to 70 km) even for adjacent cells. The light parts of the cells (with the higher wind speed) are noticeably brighter than the surrounding sea surface (background) and have a form of patches, narrow bands along the cell edges, patches coupled with bands, or sickles. Their width is about 20–50 % of the cell size. The radar contrasts are about 3.5–5.5 dB between light and dark parts of the cells, and 2–3.5 dB between light parts and background. These estimations are in good agreement with calculations for W_s=10–15 m/s and W_c=3–5 m/s (Fig. 5). BUKHAROV *et al.* (1991) carried out model calculations of the radar contrasts between various areas of the cell to estimate values of W_c/W_s and angle β. The results of wind retrieval are given in Fig. 8. The wind characteristics on the other radar images were estimated in a similar way.

As noted above, the enhanced heat fluxes in the areas with the MCC favour to the cyclogenesis. During the radar survey cloudiness field reflected the origin stage of the cyclonic vortex on the secondary cold front. The vortex reached the stage of maximum development in 7 hrs.

4. Conclusion

The analysis of the radar images obtained by the satellite SLR during winter monsoon over the Far Eastern seas confirmed that there are diverse organized structures in horizontal wind field. The most popular structures are connected with the MCC.

Brightness (NRCS) variations of the radar images of the sea surface areas over which the MCC are observed can be explained by means of a simple model of W distribution containing constant synoptic and variable mesoscale components. The mesoscale circulation inside the cells is axisymmetrical; wind is directed to the center from the cell periphery for the closed cell and vice versa for the open cell.

The model patterns of NRCS are consistent with the brightness distribution of areas with the MCC on the radar images. It follows from calculations that the patterns of the NRCS are governed by the relation between mesoscale and synoptic flows by an angle between synoptic wind direction and a radar sensing plane. It can be used to estimate the sea surface wind characteristics (MITNIK and VIKTOROV, 1990; BUKHAROV *et al.*, 1991).

The combination of visible, infrared and radar images with contact measurements provides new opportunities to study processes in the boundary layers of the atmosphere and ocean during cold air outbreaks from Asia. These layers play an important part in formation of the daily and seasonal patterns of weather and climate of the Far Eastern seas. Special experiments are necessary to study the air-sea system behavior during these processes. The comprehensive investigation of the response of the subsurface layer of the ocean to the quasiperiodic atmospheric disturbances is of primary importance.

Acknowledgments

The author wishes to thank Dr. M.V. BUKHAROV of the Russian Hydrometeorological Scientific Research Center for his valuable discussion of radar sensing of the ocean in areas with the mesoscale sea surface wind variability, and the anonymous reviewers for their careful examination and suggestions for improving the manuscript.

References

AGEE, E. M. (1987): Mesoscale cellular convection over the oceans. Dyn. Atmos. Oceans, **10**, 317–341.

AMBROZI, P., N. V. VEL'TISHCHEV, G. GOTZ. (1973): Utilization of evidence on mesoscale features of cloudiness in weather analysis. Gidrometeoizdat, Leningrad, 151 pp. (in Russian).

BUKHAROV, M. V., T. V. ZAKHAROVA and G. M. OZEROVA (1991): The reconstruction of near water wind in the regions with atmospheric convection based on a side looking radar imagery. Issledovanie Zemli iz Kosmosa, N 3, 26–32 (in Russian).

BURT, W. J. and E. M. AGEE (1977): Buoy and satellite observations of mesoscale cellular convection during AMTEX'75. Boundary-Layer Meteorol., **12**, 3–24.

CHAMPAGNE-PHILIPPE, M. (1989): Coastal wind in the transition from turbulence to mesoscale. J. Geophys. Res., **94**, 8055–8074.

D'ASARO, E. A. (1989): The decay of wind-forced mixed layer internal oscillations due to the β effect. J. Geophys. Res., **94**, 2045–2056.

DONELAN, M. A. and W. J. PIERSON (1987): Radar scattering and equilibrium ranges in wind generated waves with application to scatterometry. J. Geophys. Res., **92**, 4971–5029.

FEDOROV, K. N. and A.I. GINSBURG (1988): The Subsurface Layer of the Ocean Gidrometeoizdat, Leningrad, 304 pp. (in Russian).

HUH, O. K., L. I. ROUSE, Jr and N. D. WALKER (1984): Cold air outbreaks over the Northwest Florida continental shelf, heat flux processes and hydrographic changes. J. Geophys. Res., **89**, 717–726.

ISHIDA, H. (1989): Spectra of surface wind speed and air temperature over the ocean in the mesoscale frequency range in JASIN–1978. Boundary-Layer Meteorol., **47**, 75–84.

ISHIDA, H., W.V. BURT and V. MITSUTA (1984): The effects of mesoscale convective cells on the surface wind fields over the ocean. Boundary-Layer Meteorol., **29**, 75–84.

KALMYKOV, A. I., M. NAZIROV, P. A. NIKITIN and YU. G. SPIRIDONOV (1985): On regulated mesoscale structures on the ocean surface revealed by radar surveys from space. Issledovanie Zemli iz Kosmosa, (3), 41–47 (in Russian).

MASUKO, H., K. OKAMOTO, M. SHIMADA and S. NIWA (1986): Measurement of microwave backscattering signatures of the oceane surface using X band and Ka band airborne scatterometers. J. Geophys. Res., **91**, 13065–13085.

MITNIK, L. M. and S.V. VIKTOROV (editors) (1990): Radar Sensing of the Earth's Surface from Space. Gidrometeoizdat, Leningrad, 200 pp. (in Russian).

MONIN, A. S., R. V. OZMIDOV and V. T. PAKA (1987): On horizontal mesostructure of the main thermocline. Dokl. AN SSSR, **297**, 1469–1472 (in Russian).

MOORE, R. K. and A.K. FUNG (1979): Radar sensing wind over the ocean. Proc. IEEE, **67**, 1504–1521.

NUSS, W. A. and R. A. BROWN (1987): Evaluation of surface wind and flux analysis techniques using conventional data in marine cyclones. Dyn. Atmos. Oceans, **10**, 291–315.

ORLANSKI, I. and L. J. POLINSKY (1983): Ocean response to mesoscale atmospheric forcing. Tellus, **35**, 296–323.

OVERLAND, J. E. and J. G. WILSON (1984): Mesoscale variability in marine winds at midlatitude. J. Geophys. Res., **89**, 10599–10614.

PIERSON, W. J. (1983): The measurement of the synoptic scale wind over the ocean. J. Geophys. Res., **88**, 1683–1708.

PIERSON, W. J. (1990): Examples of, reason for, and consequences of the poor quality of wind data from ships for the marine boundary layer: Implications for remote sensing. J. Geophys. Res., **95**, 13313–13340.

POKHIL, A. E. (1985): On the indentification of storm wave conditions and calm zones in the Pacific Ocean from satellite cloud imagery. Meteorologiya and Gidrologiya, (12), 68–76 (in Russian).

TRUMP, C. L., S. J. NESHYBA and W. V. BURT (1982): Effects of mesoscale atmospheric convection cells on the waters of the East-China Sea. Boundary Layer Meteorol., **24**, 15–34.

VAN der HOVEN, I. (1957): Power spectrum of horizontal wind speed in the frequency range from 0.0007 to 900 cycles per hour. J. Meteorol., **14**, 160–164.

VETLOV, I. P. and N.F. VEL'TISHCHEV (editors) (1982): Manual by usage of satellite data in weather analysis and forecast. Gidrometeoizdat, Leningrad, 300 pp. (in Russian).